THE ASTROPHYSICAL JOURNAL, 464:487–497, 1996 June 10

YOHKOH OBSERVATIONS OF Fe XXVI X-RAY LINE EMISSION FROM SOLAR FLARES

C. D. PIKE, K. J. H. PHILLIPS, AND J. LANG
Astrophysics Division, Rutherford Appleton Laboratory, Chilton, Didcot, Oxon OX11 0QX, UK
A. STERLING[1]
Computational Physics Inc., 2750 Prosperity Avenue, Suite 600, Fairfax, Virginia 22031
T. WATANABE AND E. HIEI
National Astronomical Observatory of Japan, Mitaka, Tokyo 181, Japan
J. L. CULHANE
Mullard Space Science Laboratory, University College London, Holmbury St. Mary, Dorking, Surrey RH5 6NT, UK
AND
M. CORNILLE AND J. DUBAU
Observatoire de Paris-Meudon, F-92195 Meudon Principal Cédex, France
Received 1995 February 7; accepted 1995 December 27

ABSTRACT

We report on observations from the Bragg Crystal Spectrometer (BCS) on board the Japanese solar flare spacecraft *Yohkoh* showing Fe XXVI Lyα X-ray line emission at 1.78 Å. Some 75 events over a 2 yr period between 1991 December 6 and 1993 December 31 have been analyzed. The greater sensitivity of the BCS compared with previous instruments has enabled such emission to be detected from a wider group of flares than has previously been possible. The likelihood of detecting Fe XXVI lines in a flare is found to increase sharply with the electron temperature obtained from the Fe XXV line spectrum, also observed by the BCS, and with *GOES* X-ray class. The width of the $Ly\alpha_1$ line, measured after the impulsive stage, is greater than that determined by thermal Doppler broadening, but this is explained by the nonzero spatial extent of flares. Electron temperatures from the intensity ratio of a nearby feature due to Fe XXV dielectronic satellites and the Fe XXVI $Ly\alpha_1$ line are obtained from new atomic parameters from the superstructure code, details of which are described. This revises earlier calculations that have been extensively used. Comparison of these temperatures with those from the Fe XXV spectra provides evidence for a single loose grouping of flares, with the difference between the two temperatures ranging from nearly zero to about 20 MK. A "superhot" component would seem to be more or less developed according to whether the temperature difference is large or nearly zero. Flares at both extremes are examined in detail. The gradually varying part of the 14–33 keV X-ray emission for these events, as observed by the Hard X-ray Telescope on *Yohkoh*, has a hardness ratio corresponding to temperatures and emission measures similar to those from Fe XXVI line ratios, pointing to a common origin for their emission. Many of the flares studied occurred in particular active regions with great magnetic complexity, although Fe XXVI flares do not seem to be a distinct class within large X-ray flares.

Subject headings: Sun: flares — Sun: X-rays, gamma rays

1. INTRODUCTION

X-ray line emission from hydrogenic iron has been observed in exceptionally intense flares by spacecraft-borne instruments. The two Lyα lines, $Ly\alpha_1$ and $Ly\alpha_2$, due to transitions $1s\,^2S_{1/2}$–$2p\,^2P_{3/2}$ and $1s\,^2S_{1/2}$–$2_p\,^2P_{1/2}$, respectively, occur at 1.778 and 1.783 Å, and were well resolved with X-ray crystal spectrometers aboard the NASA *Solar Maximum Mission* and Japanese *Hinotori* spacecraft over the past decade, the observations being reported by Parmar et al. (1981), Tanaka et al. (1982), and Tanaka (1986).

Nearby Fe XXV satellites occur, falling to the long-wavelength side of the Fe XXVI lines. They are formed by dielectronic recombination, and their intensities relative to the Fe XXVI lines are a function of electron temperature T_e but independent of ionization fractions. The theory was originally developed for the case of Fe XXVI by Dubau et al. (1981). A relatively intense feature at 1.792 Å, sometimes called *J* and composed of several Fe XXV satellites with transitions $1s2l$–$2p2l$ ($l = s, p$), is suitable for use in measuring T_e. Using such intensity ratios during 13 very large flares with *GOES* X-ray classifications of M7 or higher, Tanaka (1986) deduced temperatures of up to 40 MK. Such temperatures are far higher than those deduced from satellite-to-resonance line ratios in the Fe XXV spectrum, typically ~20 MK at flare maximum, although for a number of events in Tanaka's sample the Fe XXVI and Fe XXV temperatures differed by much smaller amounts. It was deduced that the source of the Fe XXVI line emission in events with very high Fe XXVI temperatures gives rise to the nonimpulsive part of the observed hard X-ray emission in the energy range 17–40 keV. This provided confirmation of the existence of a "superhot" component in some flares, this component being previously observed with a balloon-borne hard X-ray spectrometer with high spectral resolution (Lin et al. 1981).

In the present work, we have analyzed flare events in data from the Bragg Crystal Spectrometer (BCS) on board the Japanese solar flare mission *Yohkoh*. *Yohkoh* was launched on 1991 August 30, while solar activity was still at a high level, and, at the time of this writing, is still returning high-

[1] Current address: Institute of Space and Astronautical Science, Yoshinodai 3-1-1, Sagamihara, Kanagawa 229, Japan.

quality data on the X-ray emission from the Sun in the form of images and spectra. The first year of operations in particular saw the occurrence of many very large flares. By the end of 1993, some 75 flares were identified as having detectable Fe XXVI line emission. These flares have X-ray intensities on the *GOES* scale that are mostly less than M7, the lower limit of Tanaka's (1986) sample. This reflects the higher sensitivity of the BCS instrument, although, because of this fact, the maximum phases of flares with larger X-ray intensities could not generally be observed owing to detector saturation. The 75 flares have been analyzed both as a group and individually. A central point of the analysis concerns the temperatures derived from both the Fe XXVI and Fe XXV spectra, from which deductions are made about the flare superhot component. In this paper we describe the instruments involved, the selection of flare events and reduction of data, and the results of the analysis.

2. OBSERVATIONS AND THEIR REDUCTION

2.1. *The HXT and BCS Instruments*

The observations used here were made by the Hard X-ray Telescope (HXT), Soft X-ray Telescope (SXT), and BCS, three of the instruments on board the *Yohkoh* spacecraft. Instrumental details are given by Kosugi et al. (1991) and in the *Yohkoh* HXT Handbook for the HXT, by Tsuneta et al. (1991) for the SXT, and by Culhane et al. (1991) and Lang et al. (1992, 1993) for the BCS.

Two of the BCS channels observe wavelength regions around 1.78 Å (including the Fe XXVI Lyα_1 and Lyα_2 lines and the Fe XXV dielectronic satellite feature *J*) and 1.85 Å (including the Fe XXV lines $1s^2$–$1s2s$, $1s2p$ and dielectronic satellites of Fe XXIV and Fe XXIII) and are the ones under discussion here. Other channels view He-like Ca (Ca XIX) and S (S XV) line emission. The BCS is a much more sensitive instrument than similar high-resolution spectrometers flown on previous spacecraft. Since the Fe XXV and Fe XXVI channels share the same detector, the Fe XXVI spectrum was not observable for certain times during unusually intense flares because the Fe XXV count rate reached a saturation level.

Solar X-rays with energy greater than 11.1 keV give rise to fluorescence of the germanium crystal, and this fluorescence forms a background to all channels. Adjustment of the detector discriminator levels, made for the first time in 1991 December, resulted in a reduction of the background level and the Fe XXVI line spectra becoming clearly observable.

2.2. *Event Selection*

The flare events included in the present analysis were selected on the basis of the total count rate in the BCS channel observing the Ca XIX resonance line. An initial selection of events was made by including all events for which the BCS observed a count rate of at least 1000 counts s^{-1} in the Ca XIX channel, corresponding to a mid-C *GOES* class. A total of 476 such events were identified for the times free of interruptions due to spacecraft night and passages through the Earth's radiation belts over the period from 1991 December 6 to 1993 December 31.

For each of these events, light curves (i.e., total count rate vs. time) for the Fe XXV channel were plotted. To investigate the occurrence of the generally very weak Fe XXVI line emission, spectra in the Fe XXVI channel were integrated over time periods, the boundaries of which were selected interactively. Where the coverage of a particular event permitted, the first spectrum chosen was from a time corresponding to approximately half of the peak intensity in the rising part of the Fe XXV channel light curve, and the last spectrum to a time just after peak intensity. Owing to the various gaps in data taking, it was not possible to be totally consistent in this. Thus, for a small number of events, the Fe XXV count rate temporarily reached saturation level, and so the integration times were chosen to avoid this period. The integration time periods ranged from less than a minute to about 20 minutes.

The reasons for selecting spectra in this way were threefold. First, it was found that, generally, as long an integration as possible would be required even to detect the presence of the Fe XXVI lines. Second, spectra in the earliest stages of most events showed great complexity owing to Doppler-shifted line components, and it was considered advisable to exclude these spectra from the current study. Third, our analyses of *Yohkoh* BCS data done as a preliminary to the present study had shown that, in all but a few of the most intense events (X or high-M *GOES* class), there was no evidence of the Fe XXVI spectrum during the declining phase of an event.

Within these chosen time boundaries for each flare, all iron channel spectra were corrected for detector dead time and then averaged, and the mean spectra saved for further analysis.

Because the BCS views the whole Sun, the wavelength–detector bin relationship depends on the source's Bragg angle and hence on its location in a north-south direction on the Sun. For the BCS channels viewing the Fe XXV and Fe XXVI lines, the displacement of a source from Sun center gives rise to a wavelength shift of the same sign. Because there is a fixed wavelength interval between the Fe XXV and Fe XXVI channels, there is a directly scalable relationship between the bin locations of the Fe XXV and Fe XXVI spectral lines. This has a practical application in the sense that the detector bin location of the Fe XXVI spectrum can be predicted from the observed location of the Fe XXV *w* line. Using a relationship derived from observations of some of the stronger Fe XXVI spectra, it was therefore possible to indicate the detector bin position of the chief lines expected in the Fe XXVI channel wavelength region on the spectral plot. These include the Fe XXVI Lyα_1 and Lyα_2 lines at 1.778 and 1.783 Å, respectively, as well as the Fe XXV satellite line feature *J* at 1.792 Å. In addition, for flares located sufficiently far south on the solar disk, the inner-shell Kβ line at 1.757 Å enters the wavelength range of the Fe XXVI channel. (This line, due to fluorescence-excited photospheric iron, is discussed by Phillips et al. 1994.)

As indicated in § 2.1, adjustment of the BCS discriminator levels resulted in a reduction of the crystal fluorescence background in the iron channels but did not eliminate it. The majority of this background emission was removed by subtracting a linear function, defined interactively, that approximated the background from each Fe XXVI channel spectrum. An example of a stronger Fe XXVI spectrum thus processed is shown in Figure 1.

Figure 1 illustrates a number of features occurring with these spectra generally. First, although a sloping background count has been subtracted, there still remain a number of background irregularities that resemble true lines. The cause of these has not been identified but may be

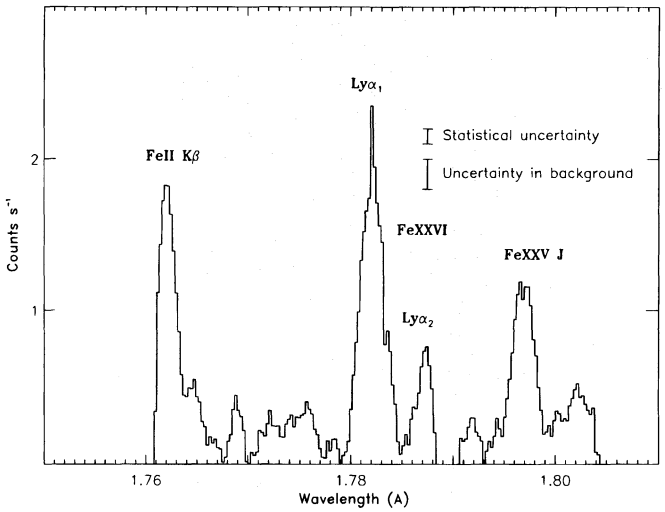

FIG. 1.—Spectrum from channel 1 of the *Yohkoh* BCS for a 3 minute interval (04:56:06–04:59:27 UT) near the peak of a large flare on 1991 December 16. The Lyα_1 and Lyα_2 lines of Fe XXVI, the Fe XXV dielectronic satellite feature called *J*, and the Fe II inner-shell Kβ (1*s*–3*p*) line appear strongly. The two error bars indicate the uncertainties due to count rate statistics and uncertainties due to background subtraction.

inherent to the detector and its on-board signal-processing techniques. Our investigations showed that they do not obviously correlate with integration time, strength of background, or real line features. It is these irregularities that set the limit of detectability of spectral features in the Fe XXVI channel data rather than the overall sensitivity of the instrument. Second, the center of the Lyα_1 line in Figure 1 shows a "spike" that is in fact an artifact of the signal processing (see Lang et al. 1992). Several such spikes are present in any spectrum, associated with particular bin numbers, so that the relationship of a spike to spectral features emitted by a flare changes with the flare's solar disk location. Despite the presence of the spike in Figure 1, the line flux is unaltered, so for the analysis presented here, no attempt was made to correct the observed spectra. Finally, the observed intensity ratio of the Fe XXVI Lyα_1 to the Lyα_2 line features is greater than the theoretical ratio for the Lyα_1 and Lyα_2 lines, viz., 2:1. Part of this discrepancy is due to the contribution of high-*n* Fe XXV satellite lines that converge on each Fe XXVI line; atomic calculations to be described in § 2.3 show that when these contributions are taken into account the ratio is indeed slightly more than 2:1, depending on temperature. However, most of the discrepancy appears to be instrumental since, for many of our weaker Fe XXVI channel spectra, the ratio is much larger, and in fact the Lyα_2 line is often only barely detectable above the irregular background, although the Lyα_1 line is definitely present.

Spectra in the Fe XXVI channel averaged over the integration periods of each event were analyzed by fitting Gaussian profiles to the Lyα_1, Lyα_2, and *J* line features when the line intensity was large enough for this to be done, in order to derive intensity, bin position, and width. Only those events showing a count rate in the Fe XXVI Lyα_1 line of at least 0.8 count s^{-1} were included for analysis. This final selection resulted in a list of 75 events, i.e., 16% of the 476 events originally selected.

The estimation of line intensities from Gaussian profile fits is subject to both statistical uncertainties that are dependent on total counts and uncertainties due to subtraction of the background, approximated as previously mentioned by a linear function. For the relatively strong spectrum illustrated in Figure 1, the estimated count rate in the Fe XXVI Lyα_1 line is 19.8 s^{-1}, the statistical uncertainty being small (less than $\pm$2%) compared with that due to background estimation, which we estimate (by taking the highest and lowest levels the background could reasonably be) to be $\pm$5%.

Table 1 gives data for the 75 events, including date and integration times (UT) (cols. [2] and [3]). The coordinates of Hα flares occurring nearest in time to the BCS flare, the NOAA active region number, and the *GOES* classification, all obtained from the NOAA *Solar–Geophysical Data Bulletin*, are given in columns (4)–(7) of this table. Column (8) gives the estimated count rates in the Fe XXVI Lyα_1 line.

2.3. *Electron Temperatures: New Calculations*

Electron temperatures may be derived from BCS Fe XXVI and Fe XXV spectra having good enough statistical quality. We will first discuss the theory for deriving the Fe XXVI [T_e(H)] temperatures. This theory is described by Dubau et al. (1981), but the calculations have now been extended. For the Fe XXVI 1*s*–2*p* collisional excitation coefficient, the formula of Vainshtein (1975) was used, based on the Coulomb-Born approximation, as in Dubau et al. (1981). Other calculations of the 1*s*–2*p* collisional rate coefficients are available (Walker 1974; Wakid & Callaway 1981; Aggarwal & Kingston 1993), but comparison shows that the rate coefficients of Vainshtein (1975) are at most 10% different. Collisional transfer between the 2*s* and 2*p* states can be neglected for solar flare densities, as was also done by Dubau et al. (1981). The calculation of the Fe XXV satellites has been revised, in particular the numerous 1*snl*–2*l'nl* satellites with high *n* that converge on the Fe XXVI lines. In the revised calculation, wavelengths, autoionization, and radiative transition probabilities for the 1*snl*–2*pnl* satellites (n = 2, 3, 4, and 5) have been calculated using the hydrogenic orbitals in order to have the same choice of orbitals for the hydrogen-like and helium-like Fe ions, so that better convergence to the Fe XXVI lines could be obtained. Satellites with *n* up to 20 were included. Figure 2 shows synthetic spectra in the 1.77–1.80 Å region for electron temperatures representative of those measured from previous flare Fe XXVI spectra; the Doppler temperature T_D is set equal to the electron temperature in these spectra. As was previously indicated by the calculations of Dubau et al., the intensity of the satellite feature *J* (1.792 Å) relative to the Fe XXVI lines is shown by this figure to be very sensitive to electron temperatures between 15 and 30 MK.

The temperature variation of the satellite feature *J* relative to the Fe XXVI lines was expressed as a table of values of the ratio J/(Lyα_1 + Lyα_2) in the work of Dubau et al. (1981). Here the variation is expressed by the ratio Lyα_1/J, which is plotted as a function of T_e (Fig. 3). The reason for omitting the Lyα_2 line in the ratio is the observational difficulty with this line in the BCS spectra. As the Lyα_1/J ratio varies as T_e for sufficiently large T_e, the high-temperature behavior is more easily displayed in Figure 3 than if the inverse ratio were plotted.

Tanaka's (1986) analysis of *Hinotori* flares used the original calculations of Dubau et al. (1981) to deduce temperatures T_e(H) from Fe XXVI line ratios. His values of T_e(H) therefore need to be revised. A comparison of the new and previous intensity ratio calculations shows that the values of T_e(H) derived by Tanaka (1986) for a given Lyα_1/J inten-

sity ratio would be lower by between 2 MK [$T_e(H) = 20$ MK] and 4 MK [$T_e(H) = 40$ MK] than values obtained from our new calculations. This is allowed for in the analysis that follows.

2.4. *Electron Temperatures: Observations*

The Fe XXVI temperature $T_e(H)$ was derived from those events for which the mean Fe XXVI channel spectra have significant count rates, defined to be at least 0.8 s^{-1}, in both the Fe XXVI Lyα_1 line and the Fe XXV J satellite feature. Corresponding emission measures were found from these count rates converted to fluxes and the emissivity of the Fe XXVI Lyα_1 line plus unresolved dielectronic satellites. The observed Lyα_1/J ratio was compared with the theory curve of Figure 3 to obtain $T_e(H)$. The uncertainties in these estimates are made up of those due to statistical uncertainties in the count rates and those due to background subtraction (see § 2.2). For spectra in which the Fe XXVI Lyα_1 line is weak, the statistical uncertainties dominate, but for stronger spectra (such as shown in Fig. 1), those in the background subtraction are more important. We estimated the statistical uncertainties from those in the total count rates of the Lyα_1 and J lines, while those in background subtraction were estimated from setting the background to the highest and lowest levels that were considered reasonably possible. The total uncertainty was taken to be the sum of these two uncertainties.

The Fe XXV temperature $T_e(He)$ was estimated with an interactive computer program in which intensity-scaled and broadened synthetic spectra calculated for different temperatures were placed over observed (Fe XXV channel) spectra, and the calculated spectrum giving the best fit to the intensity ratio of the Fe XXV w line to the Fe XXIV j dielectronic satellite was selected. (Satellite j is due to the transition $1s^2 2p\ ^2P_{3/2}$–$1s 2p^2\ ^2D_{5/2}$.) This technique relies on the temperature sensitivity of the j/w ratio, the theory of which is given by Gabriel (1972) and Bely-Dubau et al. (1982), and has been used in previous studies of *Yohkoh* data such as that of very impulsive flares by Feldman et al. (1994). This method is also discussed by Sterling, Doschek, & Pike (1994), who refer to it as the "simple spectral fitting method." The spectral resolution of the Fe XXV channel is such that this ratio can be estimated with reasonable accuracy, although an account must be taken of the fact that the observed line feature w includes $n \geq 3$ satellites. It is estimated that a relative accuracy of about ± 0.5 MK can be achieved, independent of the total count rates in the Fe XXV spectra. Comparison of the synthetic spectra used in the

TABLE 1

FLARES OBSERVED BY THE *YOHKOH* BCS TO HAVE DETECTABLE FE XXVI EMISSION

Event Number (1)	Date (2)	Integration Time (UT) (3)	Hα Flare		NOAA Active Region (6)	*GOES* X-Ray Class (7)	Count Rates (s^{-1})		$T_e(H)^a$ (MK) (10)	$T_e(He)^a$ (MK) (11)
			Coordinates (4)	Class (5)			Fe XXVI Lyα_1 Line (8)	Fe XXV w Line (9)		
1	1991 Dec 8	00:33:45–00:38:06	N10 E67	1F	6961	M1.6	2.3	143	25 (2.3)	18.0
2	1991 Dec 8	07:33:09–07:36:57	N09 E62	1N	6961	M2.8	8.9	599	29 (1.5)	19.5
3	1991 Dec 8	17:02:15–17:07:51	N10 E56	1N	6961	M3.4	19.9	1285	34 (1.4)	20.0
4	1991 Dec 8	20:22:33–20:24:33	N09 E57	SN	6961	M1.4	9.9	555	31 (1.9)	20.5
5	1991 Dec 9	09:36:30–09:45:30	N08 E48	1N	6961	M3.5	14.3	694	31 (1.3)	18.0
6	1991 Dec 10	08:12:42–08:15:57	N08 E36	SF	6961	M1.2	3.5	251	35 (2.5)	18.0
7	1991 Dec 11	15:04:34–15:07:28	S06 E57	1N	6966	M4.0	9.7	1280	32 (1.7)	18.5
8	1991 Dec 15	14:21:54–14:24:09	N06 W40	SN	6961	M1.0	5.6	412	24 (1.7)	19.0
9	1991 Dec 15	18:32:01–18:34:10				C8.0	3.1	622	...	20.0
10	1991 Dec 16	04:56:06–04:59:27	N04 W45	SF	6961	M2.7	19.8	1364	29 (1.4)	20.0
11	1991 Dec 18	10:25:06–10:31:33	S14 E39	SF	6972	M3.6	12.1	1179	...	20.5
12	1991 Dec 26	07:34:03–07:36:33	S16 W11	1N	6982	M2.9	7.9	683	...	20.0
13	1991 Dec 26	10:48:00–10:48:24				M4.6	15.5	1160	...	21.0
14	1991 Dec 26	21:35:50–21:46:32	S15 E25	1N	6985	M4.2	4.1	1320	30 (1.6)	19.5
15	1991 Dec 27	06:10:11–06:15:47	S18 E35	1B	6988	M2.1	2.8	746	22 (1.4)	18.0
16	1991 Dec 28	12:26:18–12:29:24	S18 W37	SF	6982	M3.3	6.7	1514	18 (1.3)	20.0
17	1991 Dec 30	23:06:24–23:09:03	S14 W34	2B	6985	M4.6	7.4	1584	...	19.5
18	1992 Jan 1	03:29:36–03:31:27	S16 W48	1N	6985	M2.8	8.1	979	32 (2.0)	21.0
19	1992 Jan 4	11:10:11–11:17:47	S18 W64	2N	6988	M1.9	1.7	250	...	17.5
20	1992 Jan 13	17:25:34–17:34:28				M2.0	1.9	623	...	19.0
21	1992 Jan 30	02:27:50–02:32:29	S02 W02	2N	7031	M1.6	2.5	417	22 (1.5)	19.0
22	1992 Feb 4	03:55:20–04:04:20	S06 W60	1N	7031	M1.6	1.9	259	22 (1.4)	17.0
23	1992 Feb 5	13:16:08–13:17:41	S15 W26	1B	7039	M2.2	3.1	691	...	18.5
24	1992 Feb 5	20:25:26–20:31:02	S15 W31	SF	7039	M3.1	10.5	577	34 (1.6)	16.5
25	1992 Feb 6	03:13:51–03:21:39	N06 W86	SN	7030	M7.6	7.5	544	26 (1.4)	...
26	1992 Feb 6	20:50:37–20:59:06				M4.1	25.7	1231	26 (1.2)	20.5
27	1992 Feb 7	11:49:57–11:59:09	S17 W50	2B	7039	M3.7	1.4	621	19 (1.4)	17.5
28	1992 Feb 9	03:00:27–03:05:24	S17 W72	1F	7039	M1.2	1.3	256	...	17.5
29	1992 Feb 15	21:29:59–21:34:05	S16 W13	1B	7056	M5.5	3.5	888	30 (1.9)	...
30	1992 Feb 17	15:40:25–15:46:01	N16 W81	SF	7050	M1.9	1.3	545	19 (1.5)	18.5
31	1992 Feb 19	03:48:23–03:56:29	N04 E82	1N	7067	M3.7	10.3	958	26 (1.3)	18.0
32	1992 Feb 19	14:44:35–14:53:50				C8.0	1.7	155	24 (1.6)	18.5
33	1992 Feb 21	03:05:57–03:23:00				M3.0	0.9	113	18 (1.3)	17.5
34	1992 Feb 26	01:36:24–01:39:27	S16 W90	SN	7073	M1.3	2.0	395	...	18.5
35	1992 Mar 15	01:52:22–02:10:55	S15 E27	2B	7100	M7.8	1.4	1075	...	17.5
36	1992 Apr 1	00:51:05–00:58:35	S10 W47	SN	7118	M5.6	4.7	1564	21 (1.3)	23.0
37	1992 May 5	20:07:22–20:15:55	S26 E44	1N	7154	M1.4	3.0	402	...	19.0

TABLE 1—*Continued*

Event Number (1)	Date (2)	Integration Time (UT) (3)	Hα Flare Coordinates (4)	Hα Flare Class (5)	NOAA Active Region (6)	*GOES* X-Ray Class (7)	Count Rates (s^{-1}) Fe XXVI $Ly\alpha_1$ Line (8)	Count Rates (s^{-1}) Fe XXV *w* Line (9)	T_e(H)[a] (MK) (10)	T_e(He)[a] (MK) (11)
38	1992 Jun 24	18:53:29–18:54:17	N10 W56	SF	7205	C3.6	1.5	94	22 (2.7)	17.5
39	1992 Jun 25	17:53:47–17:58:47	N09 W69	1B	7205	M1.4	9.2	588	29 (1.5)	17.5
40	1992 Jun 25	22:27:05–22:44:08				X3.0	1.2	81	16 (1.2)	...
41	1992 Jul 3	09:45:57–09:53:45	N14 E25	1N	7216	M2.1	6.8	432	...	18.5
42	1992 Jul 8	09:45:07–09:46:16	S12 E46	1N	7220	X1.2	5.1	681	...	...
43	1992 Jul 16	16:55:23–16:56:14	S10 W63	2B	7220	M6.8	4.6	762	19 (1.6)	...
44	1992 Jul 18	13:42:38–13:45:08	S08 W90	SB	7220	M2.0	3.5	837	16 (1.3)	18.5
45	1992 Aug 11	22:25:17–22:29:11				M1.4	7.7	658	33 (1.8)	19.
46	1992 Aug 20	09:03:39–09:07:21	N17 W27	1B	7260	M2.9	10.5	901	26 (1.5)	20.0
47	1992 Aug 20	20:32:55–20:38:52	N16 W33	1B	7260	M3.0	18.0	1175	32 (1.4)	20.0
48	1992 Aug 21	11:01:24–11:12:24	N14 W44	1N	7270	M1.0	5.5	409	26 (1.4)	19.0
49	1992 Sep 4	23:50:38–23:53:02	S06 W19	1B	7260	M2.5	2.0	848	...	19.0
50	1992 Sep 5	11:24:20–11:26:08	S08 W22	2B	7270	M4.0	3.5	570	...	19.5
51	1992 Sep 6	05:14:35–05:18:59	S10 W40	1N	7270	M2.4	2.7	785	22 (1.5)	19.0
52	1992 Sep 6	09:02:48–09:07:21	S10 W36	1N	7270	M3.3	6.4	1223	...	20.0
53	1992 Sep 6	11:47:55–11:51:16	S10 W41	1N	7270	M4.0	4.0	601	...	19.0
54	1992 Sep 6	23:37:03–23:38:12				M1.3	5.6	776	24 (1.9)	21.0
55	1992 Sep 7	08:51:44–08:59:14	S10 W54	SN	7270	M1.2	0.8	313	18 (1.7)	18.0
56	1992 Sep 9	02:06:57–02:14:06	S10 W72	1B	7270	M3.0	2.7	817	16 (1.2)	19.0
57	1992 Sep 10	22:52:07–22:56:58	N12 E41	2N	7276	M3.2	11.4	1368	36 (1.7)	21.0
58	1992 Sep 11	02:54:56–03:01:05	N17 E40	1B	7276	M1.1	2.8	255	23 (1.5)	18.0
59	1992 Oct 5	09:24:56–09:29:59				M1.8	1.8	643	...	19.0
60	1992 Oct 7	05:05:18–05:08:33	S07 E34	1B	7306	M3.1	3.2	1033	16 (1.3)	...
61	1992 Oct 19	17:55:10–17:58:19	N06 E24	1F	7315	M1.1	2.7	305	26 (2.0)	17.5
62	1992 Oct 27	01:44:57–01:48:06	S25 W18	1B	7321	M1.1	3.1	330	...	19.0
63	1992 Oct 27	07:38:38–07:40:38	S24 W20	1N	7321	M1.5	2.7	479	...	19.0
64	1992 Nov 5	06:19:20–06:21:53	S16 W90	SB	7323	M2.0	1.7	695	...	18.0
65	1992 Nov 23	20:17:36–20:28:33	S08 W89	SF	7342	M4.4	4.2	1041	19 (1.2)	20.5
66	1993 Feb 11	18:31:35–18:32:53	S04 W16	1B	7420	M2.7	15.9	1123	37 (1.7)	21.0
67	1993 Mar 12	17:51:43–18:08:31	S03 W48	3B	7440	M7.0	21.6	1187	33 (1.2)	20.0
68	1993 Jun 7	14:12:30–14:20:27	S10 W30	2B	7518	M5.4	4.3	910	25 (1.5)	22.0
69	1993 Jun 25	03:11:27–03:29:23	S06 E90	SF	7530	M5.1	2.7	1122	21 (1.2)	24.0
70	1993 Jun 27	11:17:11–11:19:44	S10 E56	2N	7530	M3.6	1.4	436	28 (2.0)	18.0
71	1993 Sep 27	12:08:06–12:13:45	N08 E90	1N	7590	M1.8	5.3	734	23 (1.2)	21.0
72	1993 Oct 9	08:08:23–08:11:11	N12 W74	1N	7590	M1.1	1.8	461	...	20.0
73	1993 Oct 9	19:12:24–19:17:57	N11 W78	3B	7590	M3.5	11.7	1023	21 (1.2)	23.0
74	1993 Oct 27	06:37:12–06:39:18	N10 E38	SN	7608	C9.4	2.4	217	30 (2.5)	18.5
75	1993 Dec 25	17:54:29–17:56:20	N07 E06	SN	7640	M1.5	5.4	835	...	23.0

[a] Estimated uncertainties in T_e(H) are given in parentheses in col. (10); those in T_e(He) are estimated to be 0.5 MK (see text).

computer program with those of Lemen et al. (1984) suggests that our values of T_e(He) are lower by about 1 MK. As well as the temperature T_e(He), the intensity (in counts s^{-1}) of the Fe XXV *w* line profile was measured from the mean Fe XXV channel spectra for each event in Table 1 through a best-fit Gaussian profile to the line. Because the uncertainty of background estimation is less of an issue for Fe XXV spectra, the Fe XXV temperatures and line fluxes are subject to smaller uncertainties than those from Fe XXVI spectra. With the Fe XXV line fluxes, and using calculated emissivities for the Fe XXV *w* line, we obtained emission measures.

The remaining columns of Table 1 give the Fe XXV line *w* count rates (col. [9]), and the temperatures T_e(H) (with their uncertainties) and T_e(He) (uncertainties equal to ± 0.5 MK) (cols. [10] and [11], respectively).

The temperatures T_e(H) and T_e(He) in Table 1 are averages over a period of time that includes the intensity maximum in the Fe XXV light curve, although, in fact, they are for practical purposes equal to the peak values. This was confirmed by analyzing spectra over much shorter periods of time for 10 events having high enough count rates for this to be possible (see § 3).

3. RESULTS AND DISCUSSION

The flare events of Table 1 were investigated as a statistical sample, and, in addition, those showing the most intense Fe XXVI line emission were studied individually in some detail. We now describe the results of these analyses.

Figure 4 shows the number distribution of the 75 events in Table 1 by total intensity (in counts s^{-1}) of the Fe XXVI $Ly\alpha_1$ line. As expected, this distribution falls off sharply (roughly exponentially) with increasing line intensity.

We investigated how flares were distributed according to the mean temperatures T_e(He) listed in Table 1. Figure 5 shows the number distribution with T_e(He) of all 476 events observed by the BCS in the period covered by Table 1 (1991 December 6 to 1993 December 31), with a count rate of 1000 s^{-1} in the BCS channel viewing the Ca XIX resonance line plus nearby satellites, compared with the distribution of the subset of 75 events having significant Fe XXVI line emission (hatched area), i.e., a count rate in the Fe XXVI $Ly\alpha_1$ line of at least 0.8 s^{-1}. Clearly, events showing Fe XXVI line emission have values of T_e(He) that are higher by about 3 MK than those without, although the distributions overlap appreciably. Figure 5 shows that events with estimated

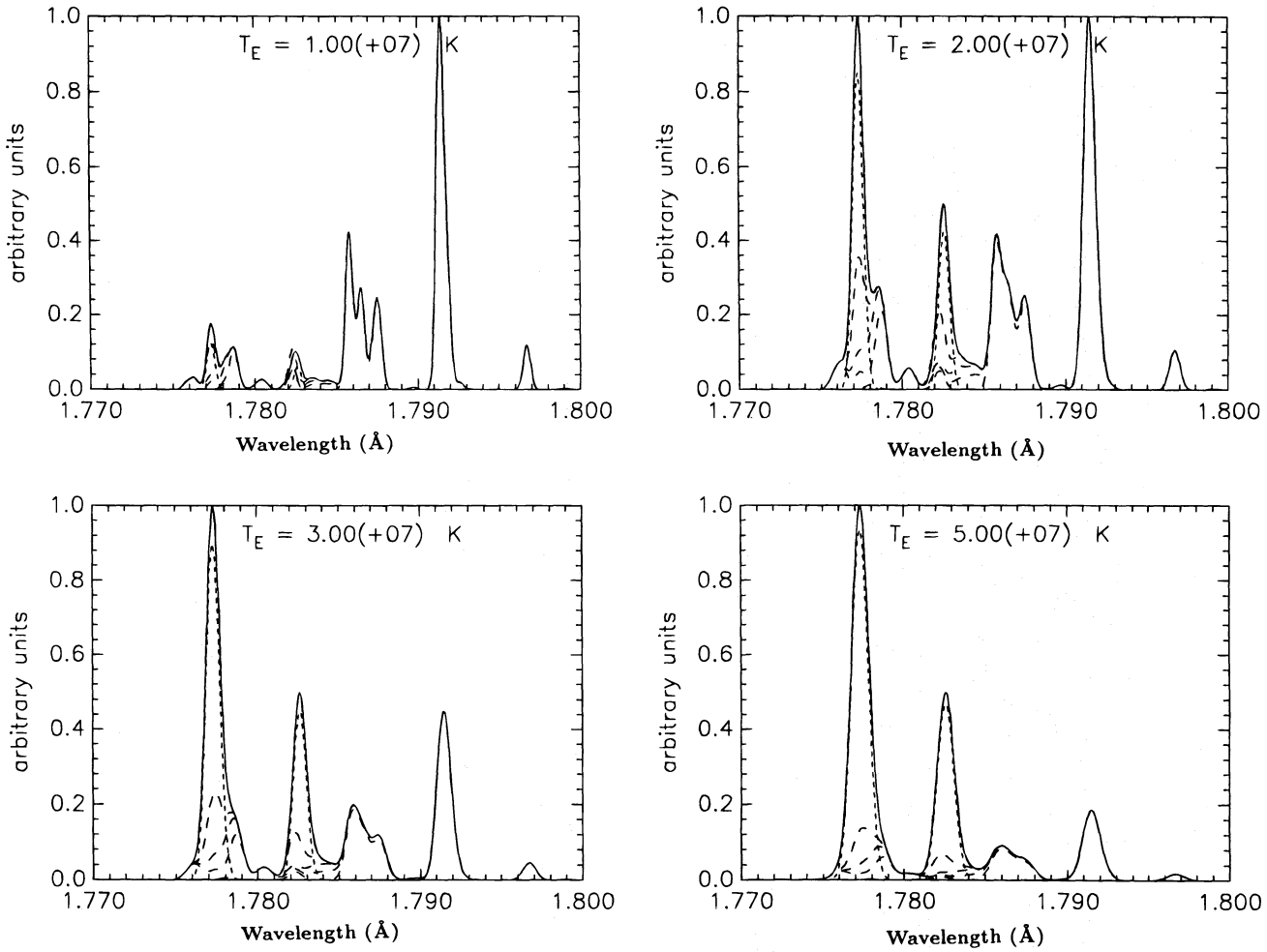

FIG. 2.—Synthetic spectra of Fe XXVI Lyα lines and nearby Fe XXV dielectronic satellites, including those blending with the Fe XXVI lines with transitions $1snl$–$2l'nl$, $l' = s$ or p and n up to 20. The calculated line intensities and wavelengths are from the SUPERSTRUCTURE code, as described in the text. The spectra are for the following electron temperatures (*from top left to bottom right*): 10, 20, 30, and 50 MK.

T_e(He) > 19 MK, almost without exception, have Fe XXVI line emission. Thus, the probability of Fe XXVI line detection rises as a simple function of T_e(He).

Of the 75 events showing Fe XXVI line emission, the majority (71) have X-ray intensities in the *GOES* classifications of M1 or greater, although one event has a *GOES* class of only C4. Thus, Fe XXVI line emission appears to rise above the detectability of our instrument (i.e., greater than 0.8 counts s^{-1} in the Lyα_1 line) at this *GOES* level. Some insight into this can be gained from Figure 5 showing how Fe XXVI line detection is related to T_e(He), and from the fact, found from our sample of 476 events having a count rate of at least 1000 counts s^{-1} in the Ca XIX channel, that there was a general increase of the Fe XXV *w* line intensity with T_e(He). Events with detectable Fe XXVI line emission are therefore likely to be associated with higher Fe XXV *w* line intensity, which in turn has a loose correlation with the 1–8 Å flux on which the *GOES* classification is based.

We investigated the widths of the Fe XXVI Lyα_1 line feature and the Fe XXV satellite line *J* in the mean spectra. The widths (FWHM) in units of Fe XXV channel detector bin widths (1 bin width equals approximately 0.000285 Å) were estimated from the Gaussian fits to the line profiles mentioned in § 2.2. The uncertainties in these estimates are about 10%. The widths (FWHM) of both the Lyα_1 and *J* lines were found to vary by over a factor of 3, from about 2–6 bins, for events in which there were significant counting rates in both lines. Figure 6*a* shows that the FWHM values of the Lyα_1 and *J* lines are strongly correlated, with the Lyα_1 line FWHM slightly larger, about 1.2 ± 0.3 times that of the *J* line. Figure 6*b* shows that the Lyα_1 line width appears to increase with increasing electron temperature T_e(H). The least-squares regression line, having a slope of 1.05, is shown in this plot (line A). Also shown is the theoretical variation of the thermal Doppler FWHM, on the assumption that the electron and Doppler temperatures are equal (line C). As already indicated, the Lyα_1 line is broadened by unresolved Fe XXV dielectronic satellites, while the *J* satellite feature is actually a blend of several $n = 2$ dielectronic satellites. Thus, both lines have widths that can be expected to be larger than the thermal Doppler width for a single line. The theoretical widths may be estimated from the synthetic spectra illustrated in Figure 2; the variation of the Lyα_1 line width (FWHM) with temperature is shown in Figure 6*b* (line B). The observed widths as defined by the regression line (line A) are between 0.4 and 1.2 bins larger than those predicted by the theory spectra over the temperature range 15–35 MK. Some of this broadening can be attributed to spatial broadening, arising from the nonzero extent of the flare emission. To check this,

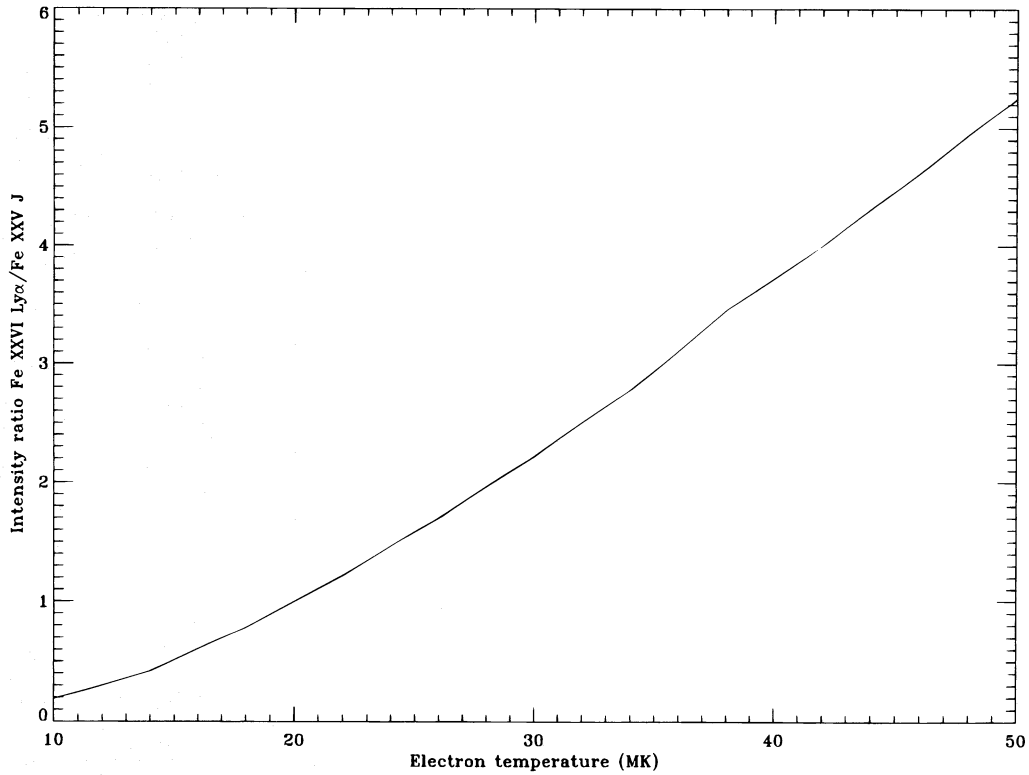

FIG. 3.—Theoretical variation with T_e of the intensity ratio of the Fe XXVI Lyα_1 line feature, allowing for close, high-n (up to $n = 20$) satellites, to the Fe XXV J line feature (wavelength 1.792 Å, composed of several dielectronic satellite lines). The calculations of line intensities used in this figure are a revised version of those of Dubau et al. (1981).

we examined images of a sample of the flares in Table 1 from the hardest filters of the SXT, sensitive to about 3–12 Å. The bulk of the emission was found to be about 2–8 SXT pixels in extent (5″–19″), exceptionally up to 20 pixels (48″). Such spatial extents along the BCS dispersion axis would give rise to a broadening in the Fe XXVI channel of between 0.3 and 2.6 bins. It is clear then that the excess broadening indicated by the differences between lines A and C in Figure 6*b* can be explained by the nonzero flare size. This possibly accounts for broadened lines reported on by Tanaka (1986) in his analysis of *Hinotori* spectra, although there attributed to turbulence.

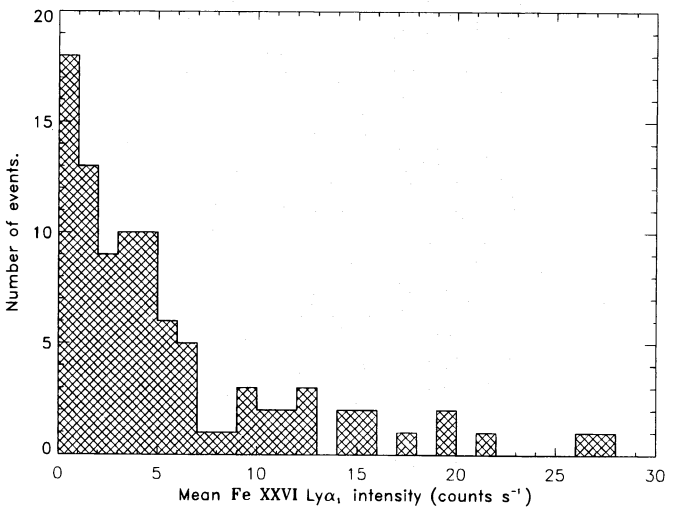

FIG. 4.—Distribution of flares for which Fe XXVI line emission was observed by the *Yohkoh* BCS, according to Fe XXVI Lyα_1 line intensity.

The derivation of single values of temperature from either the Fe XXV or Fe XXVI spectra does not imply the existence of an isothermal plasma for each flare. This point has been extensively discussed by Doschek & Feldman (1987) and Doschek et al. (1990). Doschek & Feldman (1987) consider several differential emission measure models, finding that, if T_e(H) and T_e(He) are within 3 MK, a virtually isothermal plasma is strongly implied, while the presence of a high-temperature component leads to T_e(He) being significantly increased, but with T_e(H) being substantially higher than T_e(He). Although not specifically dealt with in their analysis, it is likely that, unless a large high-temperature component were present, the total emission measure from the Fe XXVI spectrum will be less than that from the Fe XXV spectrum if T_e(H) is significantly larger than T_e(He), simply on the grounds that the differential emission measure probably declines with increasing temperature, as shown by the cases that Doschek & Feldman consider to be most realistic. Otherwise, with T_e(H) and T_e(He) having similar values, the emission measures are likely to be similar.

In Figure 7, a comparison is made of the values of T_e(H) and T_e(He) measured from the mean spectra (*filled circles*). Some 46 events are included that have measurable temperatures from both the Fe XXV and Fe XXVI spectra. It is found that the values of T_e(H) are fairly uniformly distributed between T_e(He) and a value about twice as large. As already stated, the uncertainties in the T_e(H) measurements are larger than those in T_e(He), but this does not explain the large spread of T_e(H) values for any particular value of T_e(He), which therefore appears to be real. Following the reasoning of Doschek & Feldman (1987), then, events with T_e(H) exceeding T_e(He) by a large amount are likely to be those with high-temperature components. As further confir-

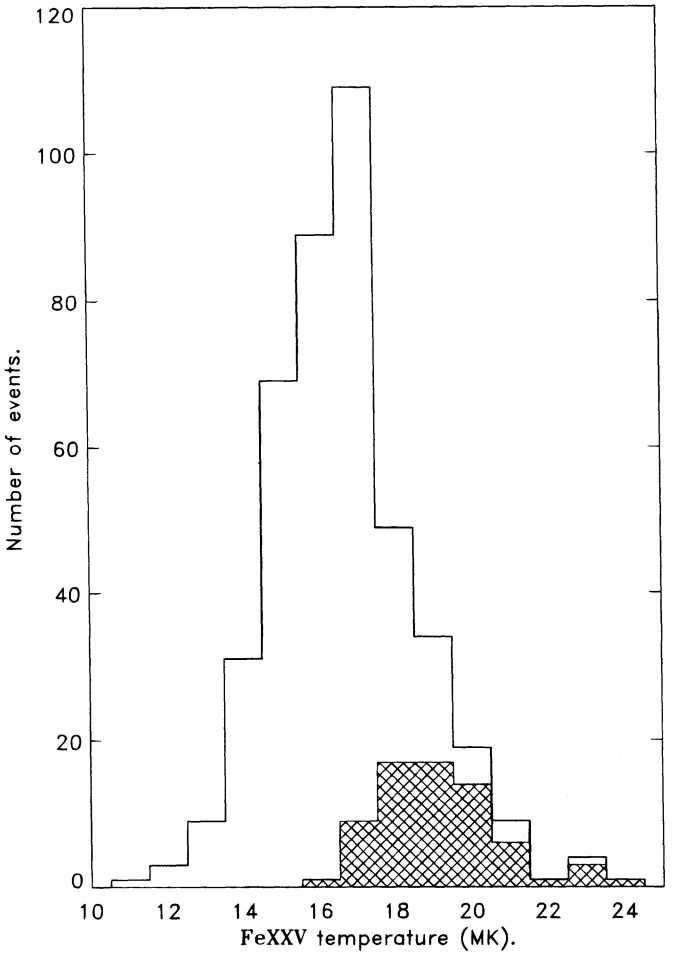

FIG. 5.—Distribution of 476 flares between 1991 December 6 and 1993 December 31 observed by the *Yohkoh* BCS to have Fe XXV line emission, according to the value of the electron temperature derived from the BCS Fe XXV spectrum [T_e(He)]. The hatched area is the distribution of the 75 flares of this sample showing, in addition, detectable Fe XXVI line emission.

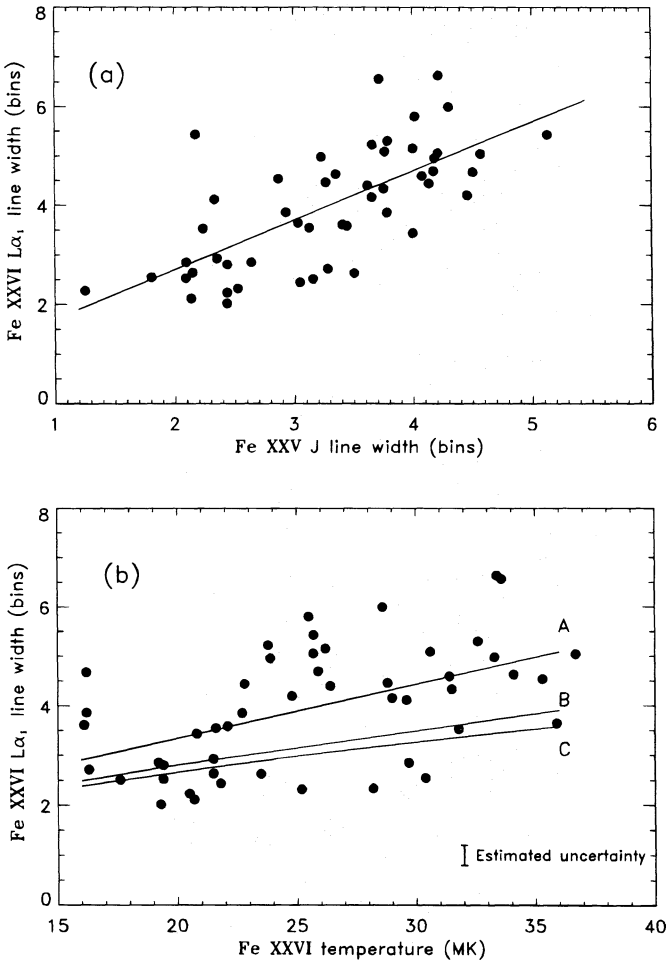

FIG. 6.—(*a*) Line width (FWHM) of the Fe XXVI Lyα_1 line feature plotted against that of the Fe XXV *J* satellite line feature, line widths being measured from mean spectra and in units of a detector bin (1 bin = 0.000285 Å). The straight line is the least-squares regression line. (*b*) Line width (FWHM) of the Fe XXVI Lyα_1 line feature plotted against T_e(H). The continuous lines are (A) the least-squares regression line; (B) the Fe XXVI Lyα_1 width (FWHM) measured from the synthetic spectra of Fig. 2; and (C) the thermal Doppler width (FWHM) on the assumption that the electron and Doppler temperatures are equal.

mation, we found that when T_e(H) exceeded T_e(He), the Fe XXVI emission measure was smaller than the Fe XXV emission measure, but the emission measures were not very different when the temperatures were similar to each other.

Figure 7 is reminiscent of the similar plot of T_e(H) and T_e(He) given for *Hinotori* events by Tanaka (1986). It was found in that study that two broad but distinct distributions of flares could be identified, one with peak T_e(H) around 22–27 MK ("low-temperature flares"), the other with peak T_e(H) exceeding 30 MK ("high-temperature flares"), with the first group having $T_e(\mathrm{H}) - T_e(\mathrm{He}) \lesssim 4$ MK and the second having $T_e(\mathrm{H}) - T_e(\mathrm{He}) \gtrsim 6.5$ MK. As mentioned, Tanaka's values of T_e(H) derived from the line intensity ratio J/Lyα_1 are lower than ours by between 2 and 4 MK (see § 2.3). Allowing for this difference, the two groups are then defined by $T_e(\mathrm{H}) - T_e(\mathrm{He}) \lesssim 7$ MK and $T_e(\mathrm{H}) - T_e(\mathrm{He}) \gtrsim 9.5$ MK. As mentioned, the *Hinotori* events were generally more intense (*GOES* class larger than M7) than ours. We have included the *Hinotori* points in the Figure 7 plot (*open circles*), the values of T_e(H) having been increased by amounts measured from the difference between Figure 3 and Tanaka's version of this plot. Figure 7 shows clearly that, rather than two flare groupings emerging, as Tanaka (1986) found, a single loose group is evident, with T_e(H)/T_e(He) ranging from 1 to 2. A superhot component, as discussed by Tanaka, is then not so much a characteristic of flares having $T_e(\mathrm{H}) - T_e(\mathrm{He})$ larger than a particular value but rather is more or less developed in a continuous manner according to whether $T_e(\mathrm{H}) - T_e(\mathrm{He})$ is large or nearly zero.

A detailed analysis of two events is summarized in Figures 8*a* and 8*b*. These events, 5 and 26 in Table 1, were chosen as among the strongest in our sample. Event 5 is representative of those with $T_e(\mathrm{H}) - T_e(\mathrm{He}) > 9.5$ MK in their averaged spectra (a "high-temperature" flare in Tanaka's 1986 terminology), and event 26 is representative of those with $T_e(\mathrm{H}) - T_e(\mathrm{He}) < 7$ MK (a "low-temperature" flare). The total count rate in the Fe XXV channel and count rates in the Fe XXV *w* and the Fe XXVI Lyα_1 line features are plotted against time. Temperatures T_e(H) and T_e(He) are also included, being derived at as many time points as possible, consistent with having good count rate statistics for each spectrum.

In § 2.4 we stated that the temperatures derived from mean Fe XXVI and Fe XXV spectra are nearly equal to peak values. This can be seen from the temperatures in Figures 8*a* and 8*b*. For these two events, the temperatures from the mean Fe XXV spectra (see Table 1) are 18.0 MK (event 5)

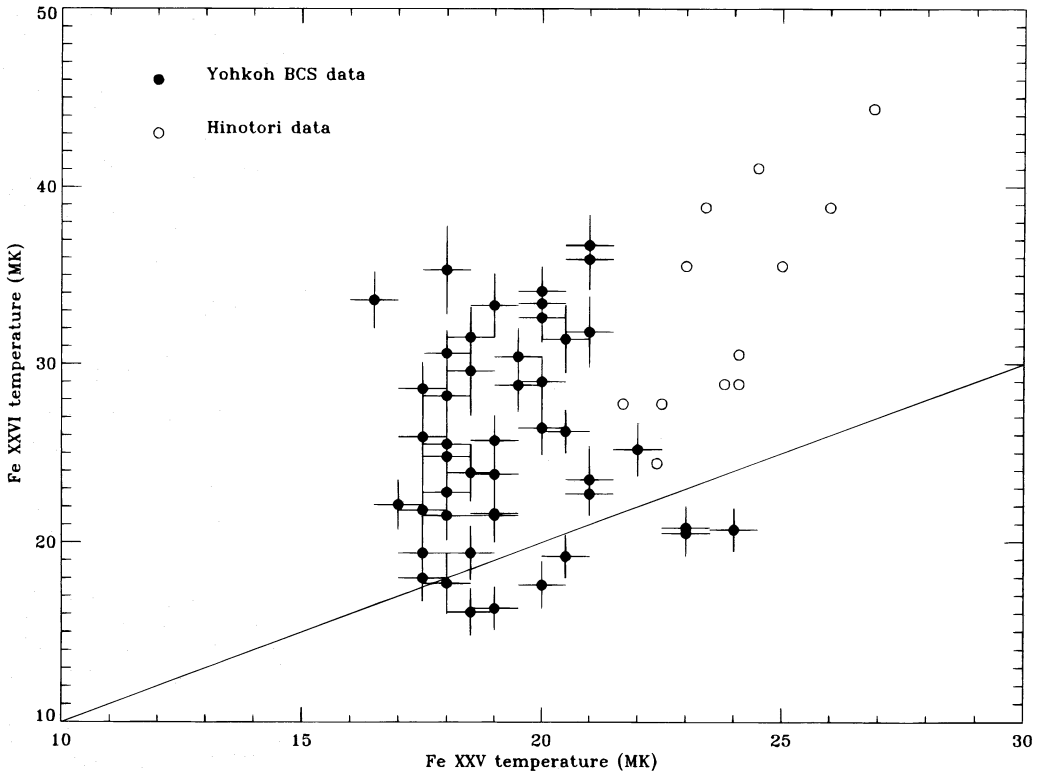

FIG. 7.—Plot of temperatures from the Fe XXVI spectrum [T_e(H)] against those from the Fe XXV spectrum [T_e(He)], both obtained from the mean spectra described in § 2.1 (*filled circles*). The uncertainties indicated by error bars are ± 0.5 MK for T_e(He) and the values indicated in Table 1 for T_e(H) (see text). Points (*open circles*) from the *Hinotori* flares discussed by Tanaka (1986) are included, his values of T_e(H) increased by between 2 and 4 MK to take into account the new atomic calculations illustrated in Fig. 3. Also shown is the line joining points with T_e(He) = T_e(H).

and 20.5 MK (event 26), while the peak temperatures (Figs. 8*a* and 8*b*) are 20.5 and 22 MK, respectively. Thus the agreement is to about 2 MK or better, justifying our earlier comment.

We examined whether a significant fraction of the hard X-ray emission as recorded by the HXT instrument from these two events was due to the superhot component as revealed by the Fe XXVI line emission observed by the BCS. The count rates in the two lowest energy channels of the HXT instrument for these flares are shown in Figures 8*a* and 8*b*. These channels are L (energy range 14–23 keV) and M1 (23–33 keV). The ratio of counting rates in the L channel to those in the M1 channel can be converted to power-law parameters (hard X-ray emission assumed to be nonthermal bremsstrahlung) or to temperature [T_e(HXT)] and emission measure (hard X-ray emission assumed to be single-temperature thermal bremsstrahlung). The computer procedures to do this, written by T. Sakao, are described in the *Yohkoh* Analysis Guide (Morrison 1994). Plots of the temperature and emission measure derived in this way are indicated in Figures 8*a* and 8*b*, the corresponding Fe XXVI points being added on the same scale.

For event 5 (1991 December 9), the HXT observations indicate that the impulsive stage—marked by rapid variations that are visible up to the M2 channel (33–53 keV)—occurred over the period 09:40–09:43 UT. The values of T_e(H) and T_e(HXT) depart significantly except for the time point at 09:44 UT, when they and the value of T_e(He) are nearly equal to one another. For event 26 (1992 February 6), the impulsive stage occurred over the period 20:51–20:59 UT, although its spectrum is too soft to register in the M2 channel. In this case, the values of T_e(H) and T_e(HXT) are within 3 MK of each other for both the impulsive and gradual phases, except for the last time point (21:05 UT), which has low statistical quality. We interpret this to mean that the gradual phase is dominated by a hot region (<20 MK), which is the source of both the HXT and Fe XXVI emission. Whether this is specifically a superhot component or not is determined by the difference between the values of T_e(H) and T_e(He), as discussed earlier.

Such a conclusion is equivalent to that from Tanaka's (1986) study from the *Hinotori* data. He found that the gradually varying part of the hard X-ray flux in the 17–40 keV range could be explained by a thermal continuum characterized by the temperature and emission measure derived from the Fe XXVI line emission, while the rapidly varying part at the time of the impulsive stage greatly exceeded that predicted from the Fe XXVI emission.

Tanaka (1986) noted that the *Hinotori* flares he classified as high-temperature generally had more gradual variations in the hard X-ray range 17–40 keV, while low-temperature flares showed more impulsive variations. We searched for such differences using the M1 (23–33 keV) range of the *Yohkoh* HXT instrument but were unable to see such a clear distinction. This is illustrated to some extent by the M1 light curves of Figures 8*a* and 8*b*, both of which have an impulsive stage near flare onset and more gradual variations later.

Finally, we investigated whether flares showing Fe XXVI line emission were associated with particular active regions having some special characteristic. It was found that certain regions produced several of the events given in Table 1, the most notable being NOAA Active Regions 6961 (eight flares) and 7270 (seven flares), which dominated solar activ-

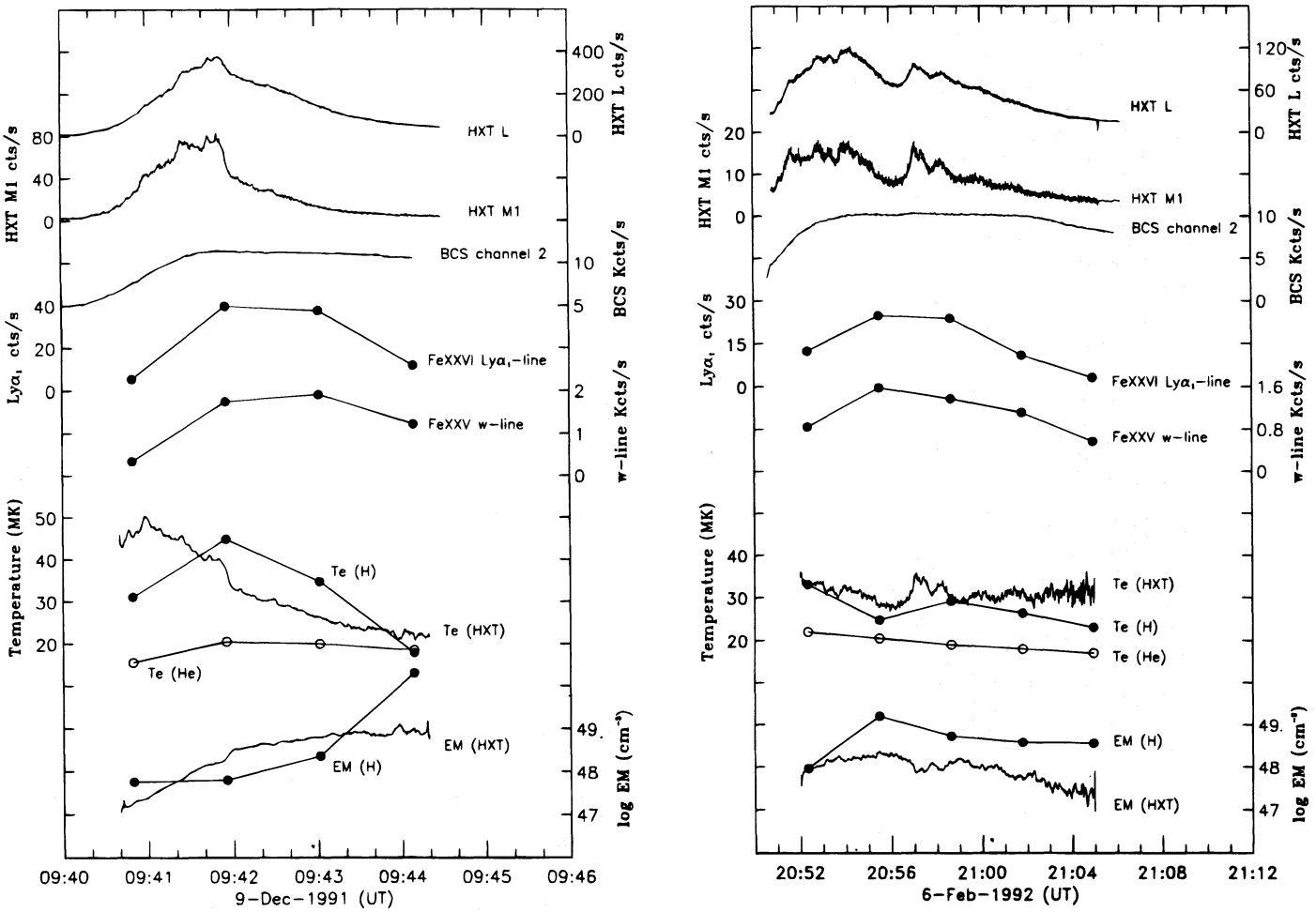

FIG. 8.—Time variations of various data for two events. From top to bottom: counts in the L and M1 channels of the *Yohkoh* HXT, the total counts in channel 2 of the BCS, counts in the Fe XXVI Lyα_1 and Fe XXV *w* line features, temperatures T_e(H) (*filled circles*, from Fe XXVI spectra) and T_e(He) (*open circles*, from Fe XXV spectra), and emission measures derived from T_e(H) (*filled circles*) compared on the same scale with temperatures and emission measures (*continuous plots*) from the HXT M1/L hardness ratio. The two events are (*a*) 1991 December 9 (peak time 09:41 UT) (event 5 of Table 1) and (*b*) 1992 February 6 (peak time 20:54 UT) (event 26).

ity in the first part of 1991 December and the first part of 1992 September, respectively. Both of these regions and most of the others listed in Table 1 showed great complexity in their photospheric magnetic field, having so-called delta configurations (the intrusion of one magnetic-polarity region into a larger region of the opposite polarity) when they were most prolific in Fe XXVI flares. However, it would seem that there is nothing to suggest that events with Fe XXVI line emission have particular characteristics, e.g., in magnetic field or Hα complexity, that distinguish them from flares that are merely large in X-ray output.

4. SUMMARY AND CONCLUSIONS

In this study, we have analyzed 75 flares showing Fe XXVI X-ray line emission, as detected with the *Yohkoh* BCS. In most cases the line emission is weak, and an averaging procedure, in which data over the rise and peak portions of each flare were integrated, was used to obtain Fe XXVI and Fe XXV spectra for detailed analysis. The greater sensitivity of the BCS has enabled us to detect Fe XXVI line emission from much weaker events than hitherto possible, although detector saturation prevented us from observing very intense events.

It was found that the likelihood of Fe XXVI line emission increases sharply with electron temperature T_e(He) as measured from line ratios in the Fe XXV spectra. Practically all flares with T_e(He) > 19.5 MK have Fe XXVI line emission that is detectable with the *Yohkoh* BCS instrument. Again, Fe XXVI line emission increases strongly with the *GOES* X-ray class, such emission becoming detectable with our instrument at *GOES* class M1.

Electron temperatures T_e(H) from the Fe XXVI spectra can be measured for most of the flares of our sample using the intensity ratio of the Fe XXV satellite feature *J* to the Fe XXVI Lyα_1 line, and atomic calculations that are a revision of the work of Dubau et al. (1981). A comparison of these with values of T_e(He) from the Fe XXV spectrum shows a continuous spread of the T_e(H)'s at a particular value of T_e(He) from T_e(He) to about $2T_e$(He). Adding points corresponding to *Hinotori* flares to the plot shows that there is a single grouping of flares rather than the two discrete groups that Tanaka's (1986) work had indicated. This points to a superhot component being a well-developed characteristic of flares having large (>9.5 MK) values of T_e(H) − T_e(He) but not otherwise. Detailed analysis of two events shows that the Fe XXVI temperatures and emission measures are similar to those from the hardness ratio M1/L from the HXT instrument, pointing to a common origin for Fe XXVI and hard X-ray emission. Such a conclusion agrees with Tanaka's (1986) work, although we could not see a clear

distinction in hard X-ray light curves for the two groups of events as was apparent in the *Hinotori* data.

Particular active regions seem prone to producing flares with Fe XXVI line emission, and such regions are characterized by great complexity in their photospheric magnetic field, in particular having delta configurations. However, there is little to suggest that Fe XXVI events form a distinct class from large flares generally.

We thank the Japanese Institute of Space and Astronautical Science who are responsible for the *Yohkoh* mission, especially Professor Y. Ogawara, and the Principal Investigators of the *Yohkoh* instruments and others in the *Yohkoh* team for their help. The Japanese activities were made possible by support of grants-in-aid for Scientific Research (03402002) and for the International Scientific Research Program (01044044). This paper is dedicated to the memory of Katsuo Tanaka (1943–90) whose pioneering work in high-temperature X-ray line emission from solar flares led to the identification of the superhot component in soft X-ray wavelengths.

REFERENCES

Aggarwal, K. M., & Kingston, A. E. 1993, ApJS, 85, 187
Bely-Dubau, F., Dubau, J., Faucher, P., & Gabriel, A. H. 1982, MNRAS, 198, 239
Culhane, J. L., et al. 1991, Sol. Phys., 136, 89
Doschek, G. A., & Feldman, U. 1987, ApJ, 313, 883
Doschek, G. A., Fludra, A., Bentley, R. D., Lang, J., Phillips, K. J. H., & Watanabe, T. 1990, ApJ, 358, 665
Dubau, J., Gabriel, A. H., Loulergue, M., Steenman-Clark, L., & Volonté, S. 1981, MNRAS, 195, 705
Feldman, U., Hiei, E., Phillips, K. J. H., Brown, C. M., & Lang, J. 1994, ApJ, 421, 843
Gabriel, A. H. 1972, MNRAS, 160, 99
Kosugi, T., et al. 1991, Sol. Phys., 136, 17
Lang, J., et al. 1992, PASJ, 44, L55
Lang, J., Brown, C. M., Magraw, J. E., & Payne, J. 1993, Rutherford Appleton Lab. Rep. RAL 93-035
Lemen, J. R., Phillips, K. J. H., Cowan, R. D., Hata, J., & Grant, I. P. 1984, A&A, 135, 313
Lin, R. P., Schwartz, R. A., Pelling, R. M., & Hurley, K. C. 1981, ApJ, 251, L109
Morrison, M. 1994, *Yohkoh* Analysis Guide, Lockheed Palo Alto Res. Lab. Rep. LMSC-P098510
Parmar, A. N., Culhane, J. L., Rapley, C. G., Antonucci, E., Gabriel, A. H., & Loulergue, M. 1981, MNRAS, 197, 29P
Phillips, K. J. H., Pike, C. D., Lang, J., Watanabe, T., & Takahashi, M. 1994, ApJ, 435, 888
Sterling, A. C., Doschek, G. A., & Pike, C. D. 1994, ApJ, 435, 898
Tanaka, K. 1986, PASJ, 38, 225
Tanaka, K., Watanabe, T., Nishi, K., & Akita, K. 1982, ApJ, 254, L59
Yohkoh HXT Handbook—I. 1993 (Tokyo: Nat. Astron. Obs.)
Tsuneta, S., et al. 1991, Sol. Phys., 136, 37
Vainshtein, L. A. 1975, Soviet Phys.—JETP Lett., 40, 32
Wakid, S. A., & Callaway, J. 1981, Phys. Lett., 81A, 333
Walker, D. W. 1974, J. Phys. B, 7, 97